[25]G. A. Baker, Jr., Advan. Theor. Phys. 1, 1 (1965).
[26]A. B. Harris, Solid State Commun. 6, 149 (1968).
[27]A recent tabulation, including a reanalysis of some of the experimental determinations of Γ_{eff} is given by A. J. Berlinsky, A. B. Harris, and C. F. Coll, III, Solid State Commun. 7, 1491 (1969).
[28]W. N. Hardy, I. F. Silvera, and J. P. McTague, Phys. Rev. Letters 22, 297 (1969).
[29]D. Ramm, H. Meyer, J. F. Jarvis, and R. L. Mills, Solid State Commun. 6, 497 (1968).
[30]D. Ramm, H. Meyer, and R. L. Mills (to be published).
[31]A. B. Harris, L. I. Amstutz, H. Meyer, and S. M. Myers, Phys. Rev. 175, 603 (1968).
[32]M. Bloom, Physica 23, 767 (1957).
[33]W. P. A. Haas, G. Seidel, and N. J. Poulis, Physica 26, 834 (1960); W. P. A. Haas, N. J. Poulis, and J. J. W. Borleffs, *ibid.* 27, 1037 (1961).
[34]L. I. Amstutz, H. Meyer, S. M. Myers, and R. L. Mills, J. Phys. Chem. Solids 30, 2693 (1969).
[35]T. Moriya and K. Motizuki, Progr. Theoret. Phys. (Kyoto) 18, 183 (1957).
[36]W. Schott, H. Rietscel, and W. Glaser, Phys. Letters 27A, 566 (1968); W. Schott (private communications).
[37]R. J. Elliott and W. M. Hartmann, Proc. Phys. Soc. (London) 90, 671 (1967).
[38]J. F. Jarvis, H. Meyer, and D. Ramm, Phys. Rev. 178, 1461 (1969).

PHYSICAL REVIEW A VOLUME 1, NUMBER 3 MARCH 1970

Pressure and Electron Density Dependence of the Electron-Ion Recombination Coefficient in Helium

Jacques Berlande, Michel Cheret, Robert Deloche, Alain Gonfalone, and Claude Manus
Service de Physique Atomique Centre d'Etudes Nucléaires de Saclay, BP n° 2, Gif-sur-Yvette, 91, France
(Received 3 October 1969)

The dependence of the recombination coefficient α of He_2^+ ions and electrons on electron density and gas pressure is measured in helium afterglow plasmas where electron and gas temperatures are equal to 300 °K, gas pressure ranges from 10 to 100 Torr, and electron density from 10^9 to 5×10^{11} cm^{-3}. Electron density decay measured by microwave interferometry is compared with computer solutions of a continuity equation for electrons which takes into account ambipolar diffusion and recombination effects. One finds $\alpha=\alpha_2+k_e n_e+k_{\text{He}}n_{\text{He}}$, where n_e and n_{He} are the electron and neutral densities, respectively, and $\alpha_2\sim5\times10^{-10}$ cm^3 sec^{-1}, $k_e=(2\pm0.7)\times10^{-20}$ cm^6 sec^{-1}, $k_{\text{He}}=(2\pm0.5)\times10^{-27}$ cm^6 sec^{-1}. These values compare satisfactorily with results of theoretical computations for a collisional-radiative recombination mechanism including both collisions with electrons and neutrals. The effect of neutrals is particularly noteworthy as far as future experimental work on weakly ionized gases is concerned.

I. INTRODUCTION

A large amount of experimental work has been devoted to the study of electron-ion recombination processes in ionized helium.

When the gas pressure is low ($p\lesssim1$ Torr), it is recognized that the three-body process $He^+ + e + e \rightarrow He^* + e$ is the main recombination mechanism if the electron density is not too low or the electron temperature too high.

When the gas pressure is higher ($p\gtrsim5$ Torr) and He_2^+ is the dominant ion, the recombination process seems more complex. A summary of the work made before 1963 can be found in a paper by Oskam.[1] Most of the experimental results were presented or interpreted in terms of a two-body dissociative mechanism. It is suggested by Ferguson *et al.*[2] that a three-body process similar to that existing at low pressure $He_2^+ + e + e \rightarrow He_2^* + e$ could more satisfactorily explain recombination rates measured in helium afterglows, the dissociative mechanism being very improbable under the experimental conditions considered. Connor and Biondi,[3] the same year, referring to the conclusions of Ferguson *et al.*, pointed out that other processes must also be present to explain some of the experimental observations. Recently Born[4] found that for $p\sim10$–20 Torr, $n_e\sim10^{12}$–10^{13} cm^{-3}, and $T_e\sim1000$–2000 °K recombination is a three-body process involving two electrons.

Bates and Khare[5] made some estimates for helium of the recombination coefficient associated with a three-body neutral stabilized mechanism, $He^+ + e + He \rightarrow He^* + He$.[6] According to these authors, for a weakly ionized helium gas (i.e., for conditions often met in previous afterglow studies), the neutral stabilized mechanism may be competitive with the electron stabilized process. It is

known that excitation transfer due to atomic collisions can be a very efficient inelastic process when the change in potential energy is small (of the order of kT_g). With regard to recombination, neutral collisions such as $He^*(p) + He \rightarrow He^*(q) + He$, $p > q$ can induce downward (toward the ground state) transitions and therefore can lead to a stabilization of the recombination process.

We have undertaken the measurement of the recombination coefficient in a helium afterglow, in the pressure range 10–100 Torr, with electron density varying from 10^9 to 5×10^{11} cm^{-3}, with $T_e \sim T_g$ in order to find any dependence of this coefficient on the gas pressure or the electron density. Simultaneously, one of us (RD) using the statistical approach proposed by Bates, Kingston, and McWhirter[7] has determined a theoretical recombination coefficient for electrons and molecular helium ions at 300 °K for different values of electron density and gas pressure.

In the following sections, we describe the microwave apparatus used for the measurement of electron density decay in helium afterglows; this decay is analyzed in terms of recombination and ambipolar diffusion rates as a function of gas pressure. Recombination coefficients are obtained. Results are compared with our own theoretical estimate, and finally with results of other investigators.

II. PRINCIPLE OF THE EXPERIMENT

A. Measurement of the Electron Density Decay

After removal of the external ionizing source, the decay of a particular average electron density in the experimental chamber is measured by microwave interferometry (X band). The chamber is a pyrex cylinder, terminated by conically tapered ends, placed in a microwave guide along its axis. The inside section of the guide is 3×3 cm. A simplified block diagram of the interferometer is shown in Fig. 1. The inside diameter of the experimental vessel is 1.84 cm, much smaller than the untapered length (30 cm).

The theory of the interpretation of plasma characteristics through the use of guided microwave propagation technique has been described in the literature,[8] and will not be detailed here. An average electron density $\langle n_e(t)\rangle_{av}$ may be deduced from the directly measured microwave absorption $A(t)$ and relative phase shift $\Delta\varphi(t)$ caused by the presence of the plasma. Assuming a cylindrical symmetry and neglecting end effects, the electron density $n_e(r, t)$ at a distance r from the axis can be expressed, whatever the position along the axis, as

$$n_e(r, t) = [n_e(r = 0, t)]\,[D_e(r, t)] \quad , \tag{1}$$

and

$$\langle n_e(t)\rangle_{av} = [n_e(r = 0, t)]\,[F(t)] \quad , \tag{2}$$

with $F(t) = \int_S D_e(r, t)E^2\,dS / \int_S E^2(r)\,dS$.

$E(r)$ is the probing microwave electric field at a distance r from the axis. The integrations are carried over the microwave guide section S.

B. Analysis of the Electron Density Decay

We suppose that the main processes which govern the variation of electron density during the afterglow are ambipolar diffusion and electron-ion He_2^+ recombination. This assumes that all volume electron-production processes, such as metastable-metastable ionization, are negligible. Therefore, one obtains

$$\frac{\partial n_e}{\partial t} = D_a \nabla^2 n_e - \alpha n_e n(He_2^+) \quad , \tag{3}$$

where D_a is the ambipolar diffusion coefficient for He_2^+ ions; α is the recombination coefficient; and $n(He_2^+)$, the He_2^+ ion density, is assumed to be equal to the electron density, since it is known that He_2^+ is the predominant ion under these conditions (see Secs. IV A and IV C).

Electrons, ions, and neutrals are considered to be at the same temperature, equal to the ambient temperature (see Sec. IV B).

Since we are looking for the effect of the electron and neutral densities on the recombination coefficient, we have chosen to write α as the sum of three terms

$$\alpha = \alpha_2 + k_e n_e + k_{He} n_{He} \quad ,$$

representing, respectively, the contribution of a "two-body," an electron-assisted, and a neutral-

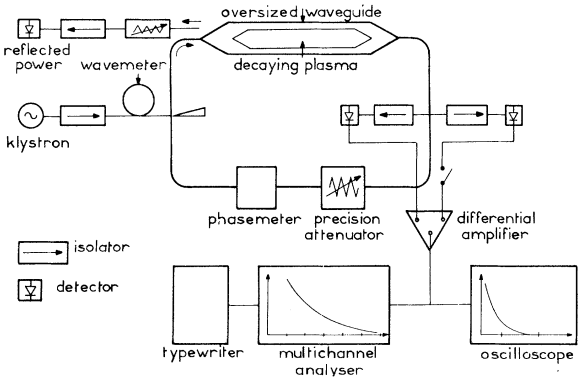

FIG. 1. Simplified block diagram of the microwave interferometer.

assisted mechanism. α_2, k_e, and k_{He} are constants depending only on the electron and gas temperature. We shall see (Sec. IIC) that this expression for α is in agreement with results of a theoretical computation.

If $\alpha_0 = \alpha_2 + k_{\mathrm{He}} n_{\mathrm{He}}$, Eq. (3) becomes

$$\frac{\partial n_e}{\partial t} = D_a \nabla^2 n_e - \alpha_0 n_e^2 - k_e n_e^3 \ . \qquad (4)$$

Sayer and Berlande[9] have developed a computer program to obtain solutions of Eq. (4) for geometries having cylindrical symmetry. One needs to know the initial value of n_e and its spatial distribution: (a) The spatial distribution $D_e(r, t=0)$ is determined by optical means. The beginning of the afterglow is not at time $t=0$, which corresponds to the start of the measurement of electron density (see Sec. IV B); (b) the electron density $n_c(r=0, t=0)$ is deduced from microwave measurements according to Eq. (2).

At a given temperature, knowing D_a and treating α_0 and k_e as parameters, the program is used to calculate first $n_e(r, t)$ then, according to Eq. (2), $\langle n_e(t) \rangle_{\mathrm{av}}$ for comparison with our measurements. The desired coefficients α_0 and k_e are taken as those resulting from a good fit between an experimental and a computed curve.

C. Theoretical Considerations on Electron-Ion Recombination in a Weakly Ionized Helium Gas

As mentioned in Sec. I, Deloche, using the statistical approach proposed by Bates, Kingston, and McWhirter,[7] has calculated the electron-He_2^+ ion recombination coefficient associated with a collisional-radiative mechanism, where both electron and neutral collisions are included. Therefore, the following processes were considered in the calculations:

$$He_2^+ + 2e \rightleftarrows He_2^*(p) + e \ , \qquad (5a)$$

$$He_2^+ + e + He \rightleftarrows He_2^*(p) + He \ , \qquad (5b)$$

$$He_2^+ + e \rightarrow He_2^*(p) + h\nu \ , \qquad (5c)$$

$$He_2^*(p) + e \rightleftarrows He_2^*(q) + e, \quad p > q \qquad (5d)$$

$$He_2^*(p) + He \rightleftarrows He_2^*(q) + He, \quad p > q \qquad (5e)$$

$$He_2^*(p) \rightarrow He_2^*(q) + h\nu, \quad p > q \ . \qquad (5f)$$

A simplified model of the helium molecule was adopted. Details of the calculations and rate coefficients used are given in papers by Deloche[10] and Deloche and Gonfalone.[11] The results for α are reproduced in Fig. 8 (dashed lines). α for such a mechanism can be written at 300 °K and a given pressure, as $\alpha_0 + k_e n_e$ and, more generally, for any pressure (between 10 and 300 Torr) as $\alpha_2 + k_{\mathrm{He}} n_{\mathrm{He}} + k_e n_e$. Recently, Collins[12] reached the same conclusion.

In addition to the recombination coefficient α, this theoretical approach gives the population densities of the various excited states of the simplified helium molecule. When the degree of ionization is low ($< 10^{-8}$) these densities, for the lower excited states, are proportional to the square of the electron density.

III. EXPERIMENTAL APPARATUS

A simplified block diagram of the over-all apparatus is shown in Fig. 2. Care is taken to achieve a high purity of the gas under study.

After baking, a residual pressure $\sim 10^{-9}$ Torr is reached in the experimental chamber. Before being introduced, helium is purified successively in

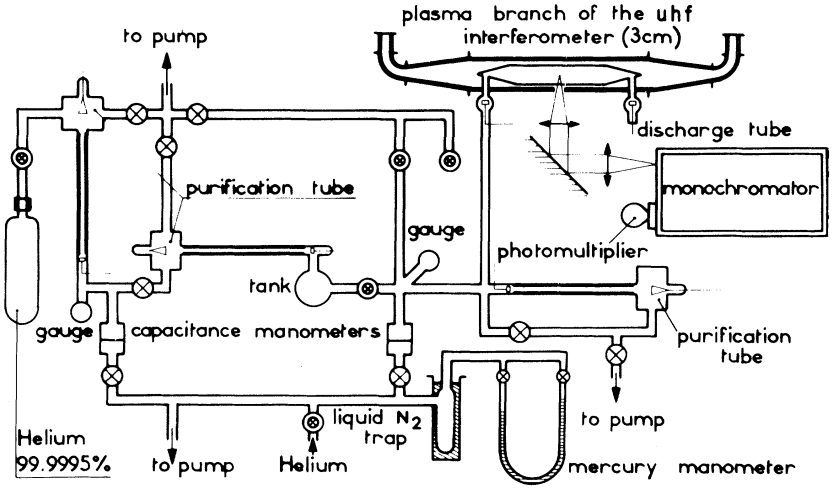

FIG. 2. Simplified block diagram of the over-all apparatus.

two watercooled cataphoresis tubes, at pressures up to 200 Torr. Impurity concentration is estimated by optical techniques to be of the order of 10^{-8}. Helium is introduced by means of a variable leak in the discharge chamber, and its pressure measured by a capacitance manometer. A third cataphoresis tube directly connected to the chamber is intended to trap the impurities which could be desorbed, during the different phases of measurement, from the walls and electrodes of the chamber. The gas is ionized by high-voltage dc pulses; the length of the pulses is adjustable from 10 μsec to 5 msec, and their repetition rate is variable between 1 and 100 per second. The reproducibility of the discharge is excellent. Typical operating conditions for the discharge are

duration: 100 μsec ,
repetition rate: 20 sec^{-1} ,
average intensity: 100 mA .

These values have been chosen in order to avoid any heating of the gas and yet have a stable discharge.

The light emitted by the ionized gas is observed through various small holes and slits drilled in the waveguide. This light is analyzed by a double monochromator and detected by a cooled photomultiplier and a multichannel analyzer (Intertechnique Didac 800).

The microwave interferometer includes a precision attenuator to measure the absorption $A(t)$, and a calibrated phasemeter to determine the relative phase shift $\Delta\varphi(t)$. For small values of $\Delta\varphi(t)$, a differential technique and the use of a multichannel analyzer make possible the measurement of phase shift down to 0.01 deg with a 10% precision. The average electron density can therefore be determined over a very large range.

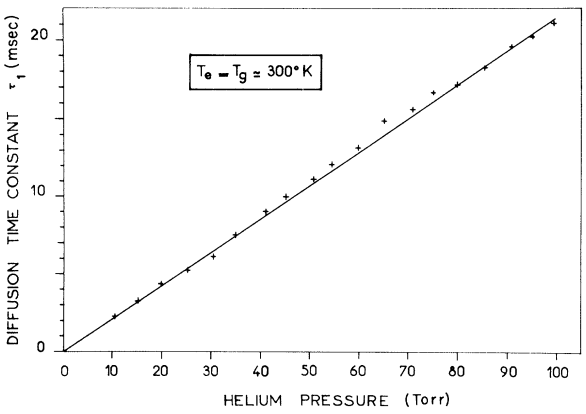

FIG. 3. Measured ambipolar diffusion time constant τ_1 as a function of gas pressure.

IV. MEASUREMENTS AND RESULTS

A. Ambipolar Diffusion

Due to the high sensitivity of the microwave interferometer, electron density can be measured in the very late afterglow, where the diffusion is dominant loss mechanism for electrons. The diffusion time constant τ_1 in the fundamental mode is determined in this manner with good accuracy. Between 10 and 100 Torr, τ_1 is proportional to the gas pressure (see Fig. 3), which indicates no appreciable change in the type of ion in this pressure range: the calculated mobility is 16.1 ± 0.8 cm^2 $\text{V}^{-1}\text{sec}^{-1}$ at 300 °K. This result together with optical observations (Sec. IV C) and findings of other investigators[13] seems to indicate a predominance of He_2^+ ions in the afterglow.

B. Electron and Gas Temperature

As mentioned earlier, time $t = 0$ corresponding to the start of electron density measurement is situated, for most of the experiments, 900 μsec after the end of the voltage pulse (900 μsec into the afterglow).

Electron temperature is not measured in our experiments, but it is reasonable to assume for these high pressures that electrons at time $t = 0$ have a Maxwellian distribution at the gas temperature. Recent radiometric measurements made in similar experimental conditions by Delpech[14] show, for a pressure of 23 Torr, a thermalization time of the order of 50 μsec.

The mean rise of gas temperature due to the electric power dissipated during the discharge is deduced from the slight increase of pressure observed when the discharge is turned on. At 20 Torr, for a discharge repetition rate of 20 per sec and an intensity of 100 mA, this rise is less than 1 °C.

C. Optical Observations and Measurements

The electron spatial distribution $D_e(r, t = 0)$ at time $t = 0$ has been determined for each value of the pressure by optical techniques. Using a multichannel analyzer, we measure the variation of the intensity of a spectral band emitted by the plasma perpendicular to the axis of the cylindrical experimental chamber. The radial distribution of the emitting molecules is obtained by Abel inversion. The radial electron distribution is deduced assuming that, in the range of neutral and electron densities we are considering, the population densities of the lower excited states of the helium molecule are proportional to the square of the electron density. This is justified by the following considerations: (i) Previous experimental work[15] and mea-

surements in our laboratory have shown such a square dependence for the total light emitted at some wavelength either from the side or the end of the discharge chamber without any spatial resolution, upon the average electron density $\langle n_e(t)\rangle_{av}$. To make sure that the inversion technique is valid, measurements of the distribution were made in the late afterglow; at that time one obtains the correct zero-order Bessel function; (ii) Theoretically, as mentioned in Sec. II C, the dependence of excited-state populations upon electron density approaches a square law when the pressure increases.

It is clear that only approximate shape for the electron spatial distribution is obtained here. However this is not important since we do not need a very high precision for this shape. As a matter of fact the computer solutions of Eq. (4) are not affected by small variation of the initial distributions, as noted by other investigators.[16]

We checked that the symmetry of the plasma in different sections of the chamber is really cylindrical which is essential for comparison of experimental data with computer solutions of Eq. (4).

Finally it was noted that, under our experimental conditions, helium afterglows emit mainly band spectra, typical of excited molecular helium; this would indicate a predominance of He_2^+ ions, giving He_2^* after recombination.

D. Electron-Ion Recombination

We may now compare experimental data and the computer solutions of Eq. (4). Figures 4–6 show the variation of $\langle n_e(t)\rangle_{av}/n_e(r=0,\ t=0)$ as a function of t/τ_1 at a given pressure (these coordinates were used for convenience in the computations). Computer solutions, for different values of α_0 and k_e, are represented by solid lines; the circles are the experimental data. The computed curves and the experimental data are generally compared over the range $0 < t/\tau_1 < 2$, since the ambipolar diffusion rate begins to predominate the recombination rate for $t/\tau_1 > 2$, and the comparison loses its interest for our purposes. It can be seen however in Fig. 4, that the fit between a particular computed curve and the experimental data is good over the whole range of electron density measurement, which corresponds to eight time constants in this case.

The precise value of the coefficient k_e from $\alpha = \alpha_0 + k_e n_e$ has been determined at 10.8 Torr. It is found that $k_e = (2 \pm 0.7) \times 10^{-20}$ cm^6 sec^{-1} with $\alpha_0 = 1 \times 10^{-9}$ cm^3 sec^{-1}. In Fig. 4, α_0 is constant and equal to 1×10^{-9} cm^3 sec^{-1}, and k_e is varied. Changing α_0 has a different effect on the shape of the computed curves to changing k_e, making unequivocal the determination of these coefficients. We have found that the best fit between experimental and computed curves occurs at each pressure for the same value of k_e, although the determination of k_e becomes less and less precise as the pressure increases.

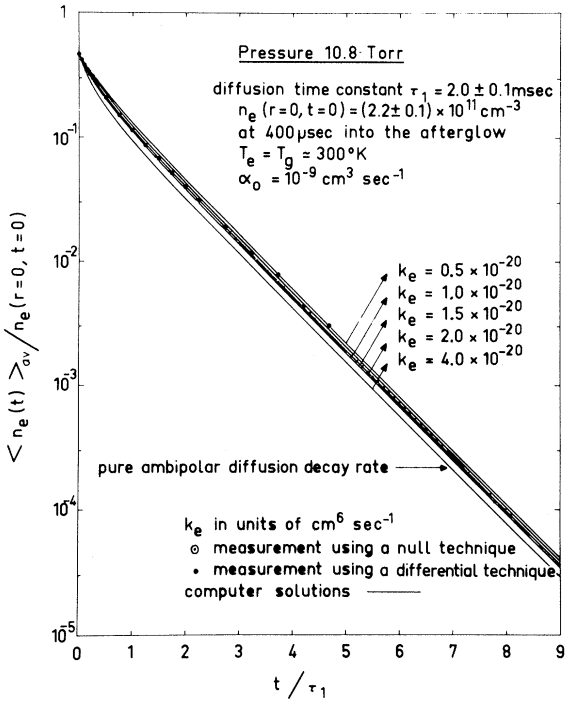

FIG. 4. Variation with time into the afterglow of the experimental average electron density (open circles) compared with computer solutions of Eq. (4) (solid lines). For convenience, reduced coordinates are used (see details in the text).

In Figs. 5 and 6, computer solutions (α_0 being treated as a parameter) and experimental data are compared at different values of pressure, for a constant k_e. If the fit, for particular values of α_0, is very good in the pressure range 10–60 Torr, a slight disagreement appears over 60 Torr; this disagreement cannot be eliminated by changing the values of α_0 and k_e or the form of the initial spatial distribution when Eq. (4) is solved. This disagreement increases with pressure. Although we are not able at the present to provide an explanation for this, we think it could be due to some secondary-effect phenomena, such as metastable-metastable ionization. This point is presently under study experimentally and an electron production term is introduced into Eq. (4). The value of α_0 at 80 and 100 Torr has therefore been determined during the early part of the afterglow ($t < 0.3\tau_1$), where the influence of the secondary effect has been assumed to be negligible.

We have checked that the value of the discharge current has no influence on the determination of α_0 and k_e. At 20 Torr, for current intensities ranging from 10–300 mA (higher currents would heat the

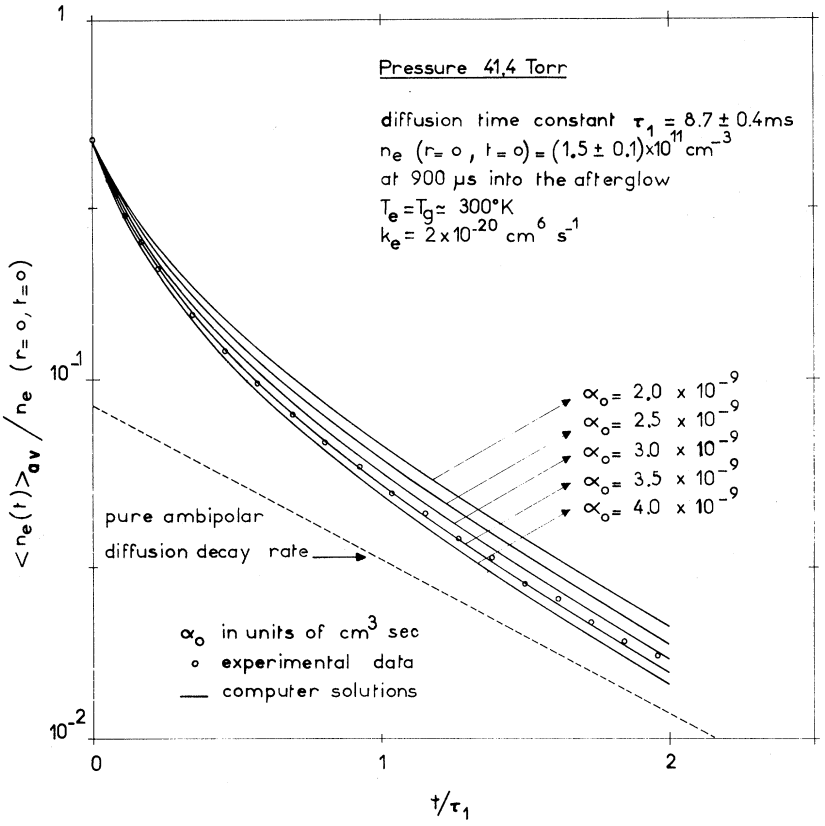

FIG. 5. Variation with time into the afterglow of the experimental average electron density (open circles) compared with computer solutions of Eq. (4) (solid lines). For convenience, reduced coordinates are used (see details in the text).

gas and cause some desorption from the walls), the fit between experimental and computed curves is best for exactly the same value of α_0 and k_e (within experimental uncertainties) even though these intensities correspond to quite different initial conditions.

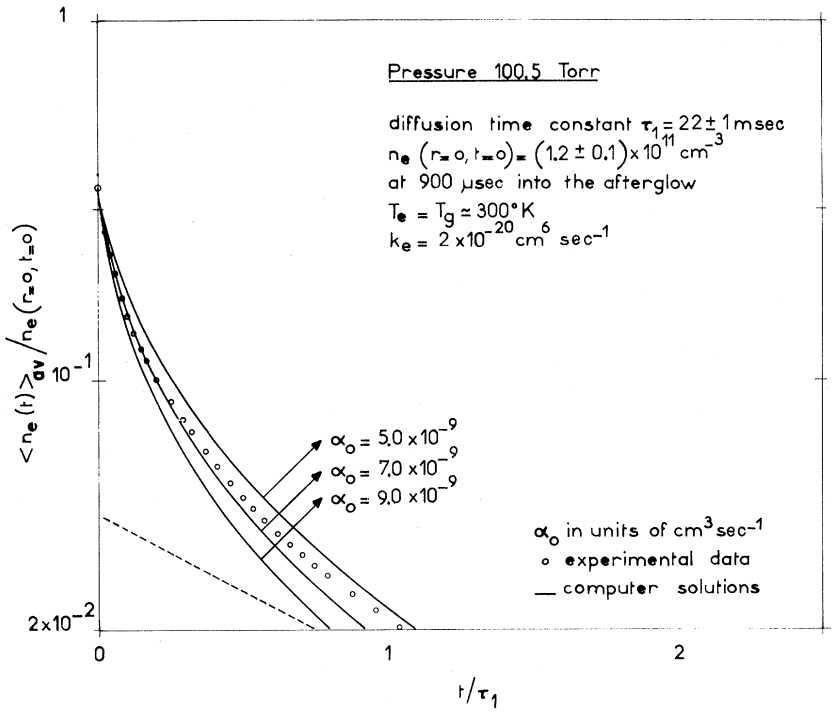

FIG. 6. Variation with time into the afterglow of the experimental average electron density (open circles) compared with computer solutions of Eq. (4) (solid lines). For convenience, reduced coordinates are used (see details in the text).

The variation of $\alpha_0(\alpha_0 = \alpha_2 + k_{He} n_{He})$ with pressure is shown in Fig. 7. Open circles are experimental data for $k_e = 2\times10^{-20}$ cm^6 sec^{-1}. Points are situated on a straight line, giving $k_{He} = 2\times10^{-27}$ cm^6 sec^{-1} and $\alpha_2 = 5\times10^{-10}$ cm^3 sec^{-1}. Taking into account the error in k_e (outside lines in Fig. 7), one finds

$$k_{He} = (2 \pm 0.5)\times10^{-27} \text{ cm}^6 \text{ sec}^{-1} \quad ,$$

and $$\alpha_2 = (5 \pm 2)\times10^{-10} \text{ cm}^3 \text{ sec}^{-1} \quad .$$

The measurements have not been extended to pressures lower than 10 Torr, as we wanted to be sure that He_2^+ was the predominant ion during the afterglow. The error in the value of α_0 is 25%, and that in k_e is 35%, taking into account the experimental uncertainties and the sensitivity of the comparison technique we have used.

V. DISCUSSION AND CONCLUSIONS

With some restrictions at high pressures, the electron density decay in helium afterglows may be analyzed in terms of ambipolar diffusion and recombination rates if one considers that the recombination coefficient α depends upon the electron and neutral densities, according to

$$\alpha = \alpha_2 + k_{He} n_{He} + k_e n_e \quad .$$

Undoubtedly, complex processes are present in helium afterglows at high pressures; optical observations in this laboratory have shown, apart from strong emission bands, weak helium lines that presumably indicate the existence of He^+ ions, which possibly result from metastable-metastable collisions. We think however that this would not affect the results and conclusions of this work very much.

For purely electron-assisted recombination and for $n_e > 10^9$ cm^{-3}, the recombination coefficient can be written $\alpha_e = k_e n_e$ according to the theory of Bates *et al.*[7] At 300 °K $(k_e)_{Bates} \sim 10\times10^{-20}$ cm^6 sec^{-1}. Using the complete Gryzinski formula,[17] Deloche[10] has found (see the high electron density region in Fig. 8) $(k_e)_{Deloche} = 4\times10^{-20}$ cm^6 sec^{-1}.

The result of the present experimental work is $(k_e)_{expt} = (2 \pm 0.7)\times10^{-20}$ cm^6 sec^{-1}. One may see from the difference between results obtained by Bates and Deloche that the recombination coefficient is very sensitive to the electron excitation cross sections used in the computations. Since the theoretical values of these cross sections are rather inaccurate, it is not surprising to find an ex-

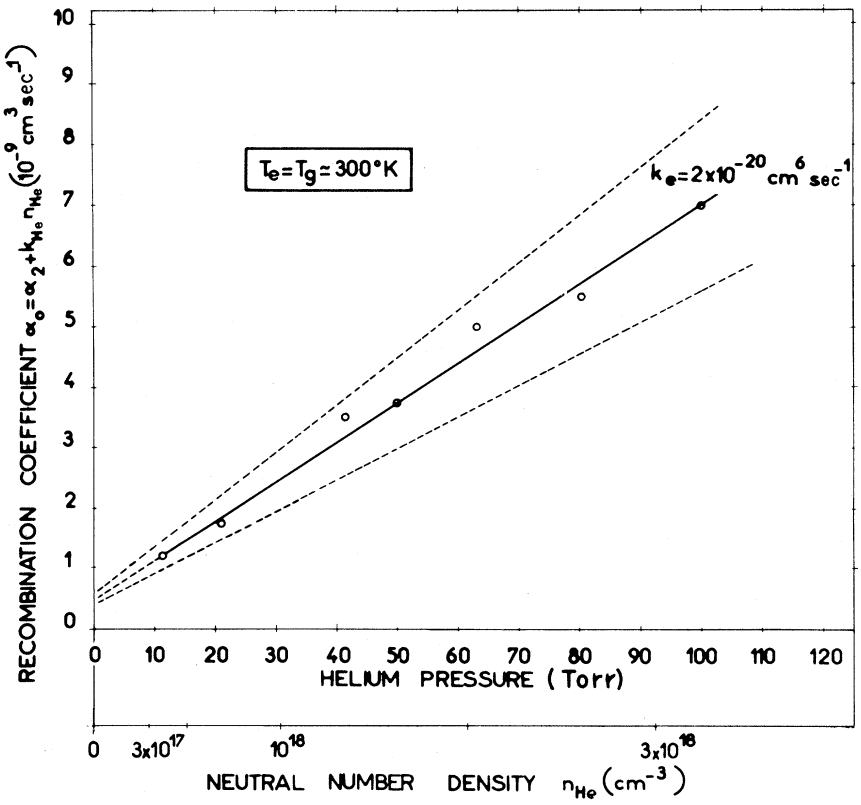

FIG. 7. Measured variation of the recombination coefficient $\alpha_0 = \alpha_2 + k_{He} n_{He}$, as a function of neutral density for $k_e = 2\times10^{-20}$ cm^6 sec^{-1} (open circles). The external lines correspond to the mean values of α_0 obtained when the error in k_e is taken into account.

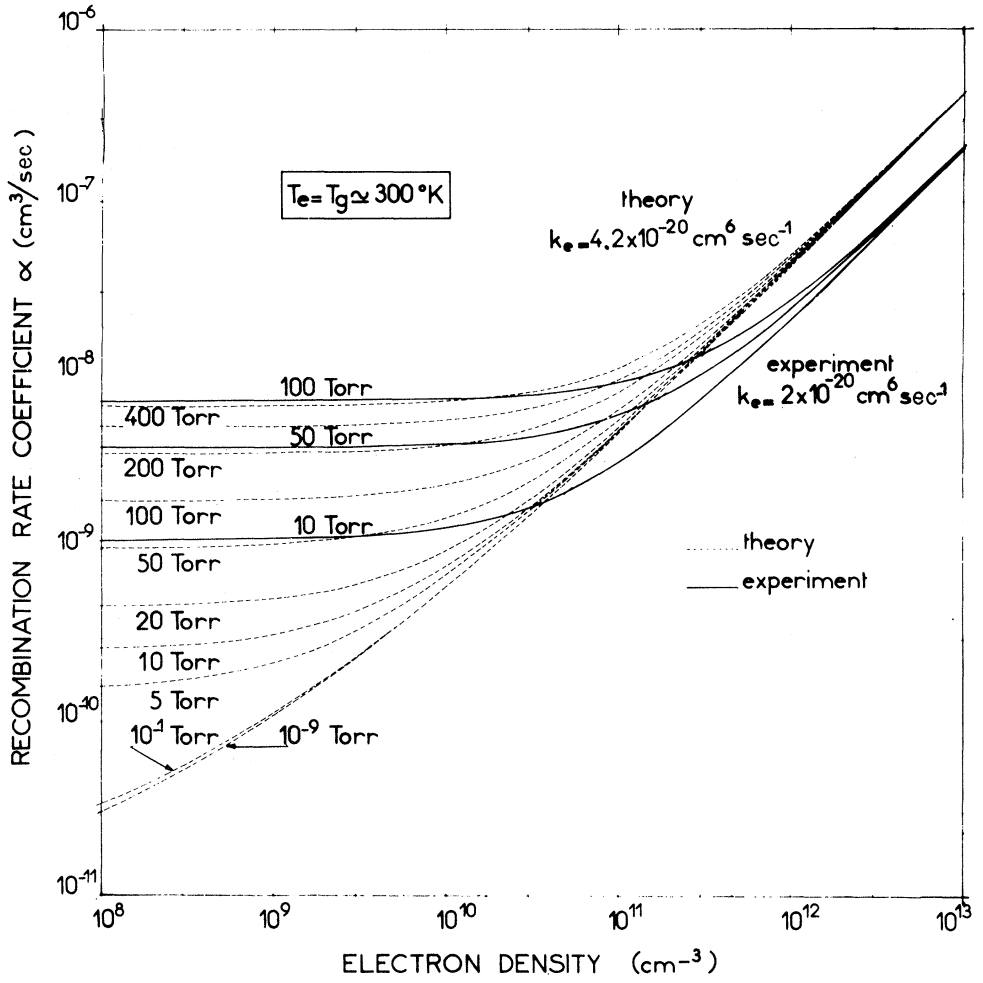

FIG. 8. Variation of the total recombination coefficient $\alpha(He_2^+)$ as a function of electron density for different values of the gas pressure. The solid lines represent the total recombination coefficient $\alpha = \alpha_0 + k_e n_e$ calculated with those values of α_0 and k_e obtained in our experiments. The dashed lines show the results of the theoretical computations performed by Deloche (See Ref. 10).

perimental value half the theoretical one.

It is interesting to note that, while at higher electron densities and temperature measurements of the electron-assisted recombination coefficient α_e are numerous, we present here the first experimental determination of α_e at 300 °K and for n_e $\sim 10^9$–10^{11} cm^3.

With regard to the coefficient k_{He}, no experimental evidence of a dependence of the recombination coefficient on gas pressure exists in the literature.[18] Theoretical calculations by Bates and Khare[5] for purely neutral-assisted recombination, and by Pitaevskii,[19] indicate

$$k_{He} = 1\times10^{-27}\ \text{cm}^6\,\text{sec}^{-1}\ \text{(Bates)}, \qquad 300\,^\circ\text{K}$$

$$k_{He} = 2.5\times10^{-27}\ \text{cm}^6\,\text{sec}^{-1}\ \text{(Pitaevskii)}, \quad 300\,^\circ\text{K}.$$

The Thomson theory,[20] modified for electron-ion recombination, gives

$$k_{He} = 4\times10^{-28}\ \text{cm}^6\,\text{sec}^{-1}, \quad \text{at } 300\,^\circ\text{K}\ .$$

Our theoretical result, deduced from the low electron density region in Fig. 8, is $k_{He} = 5.3 \times 10^{-28}$ cm^6 sec^{-1}, using a very approximate formula for neutral induced excitation rates.[21] The agreement between the experimental result $k_{He} = (2 \pm 0.5)\times10^{-27}$ cm^6 sec^{-1} and the theoretical values can therefore be considered good.

Finally, a "two-body" recombination coefficient $\alpha_2 = 5\times10^{-10}$ cm^3 sec^{-1} has been obtained by extrapolation of data to zero pressure (see Fig. 7). If the theoretical values for α (Fig. 8) are written $\alpha_{theor} = (\alpha_2)_{theor} + (k_e)_{theor} n_e + (k_{He})_{theor} n_{He}$

with $(k_e)_{\text{theor}} = 4\times10^{-20}$ cm^6 sec^{-1} and $(k_{\text{He}})_{\text{theor}} = 5.3\times10^{-28}$ cm^6 sec^{-1}, one finds a value of the order of 2×10^{-10} cm^3 sec^{-1} for $(\alpha_2)_{\text{theor}}$. This can be considered as a theoretical estimation for α_2 to be compared with the experimental result; however, the error in both the experimental and the theoretical coefficient is such that no conclusion can be drawn concerning their respective values.

Our results are summarized in Fig. 8, using the gas pressure as a parameter. Full lines represent, as a function of electron density, the total recombination coefficient according to $\alpha = \alpha_2 + k_e n_e + k_{\text{He}} n_{\text{He}}$, where the constants α_2, k_e, and k_{He} are given values obtained in these experiments.[22] The curves are drawn for a larger range of electron density than is considered in the experiment (10^9–5×10^{11} cm^{-3}). In the same figure, the results of the theoretical computations performed by Deloche[10] are plotted for comparison (dashed lines).

As noted in Sec. I, a large amount of experimental work has been devoted to the study of electron-ion recombination in high-pressure helium afterglows at 300 °K, but no mention has ever been made of a dependence of α upon gas pressure or electron density. The analysis of the afterglow has been in most cases not as elaborate as that used in the present work, and the pressure range investigated not large enough.

Considering the results of Chen *et al.*,[23] (the experimental apparatus used is very similar to ours,) and utilizing the analysis of this work during the early part of the afterglow at a pressure of 30 mm, one finds that $k_e \sim 10^{-20}$ cm^{-6} sec^{-1} and $\alpha_0 = \alpha_2 + k_{\text{He}} n_{\text{He}} \sim 3\times10^{-9}$ cm^3 sec^{-1}; our results are $k_e = (2\pm0.7)\times10^{-20}$ cm^6 sec^{-1} and $\alpha_0 = (2.2\pm0.5)\times10^{-9}$ cm^3 sec^{-1} at 30 mm. Although the comparison is good, no definitive conclusion should be drawn from this agreement, since more experimental results are needed. Furthermore, the upper limit of the recombination coefficient estimated by Oskam[1] to be 4×10^{-9} cm^3 sec^{-1} at 60 Torr, and the value 1.3×10^{-9} cm^3 sec^{-1} given by Gray and Kerr[24] in the pressure range 15–20 Torr are in good agreement with our results, for the electron density region considered by these authors.

In view of the dependence of the recombination coefficient α on the electron density and gas pressure, as found experimentally, and the agreement both qualitative and quantitative between this result and the findings by Deloche[10] and Bates[5,7], it seems beyond doubt that a collisional-radiative mechanism, where both electrons and neutrals contribute to the stabilization of the process, is the main recombination mechanism in weakly ionized helium afterglows. Although this work was mainly concerned with the determination of α from electron density decay measurements, it should be mentioned that optical observations made simultaneously during these afterglows can be explained with the theory developed by Deloche for a collisional-radiative mechanism including neutral collisions. In particular, this theory indicates that the intensity of the light emitted by the lower excited states approaches a square-law dependence on the electron density when the degree of ionization is low. Experiments seem to confirm this result.

HELIUM PRESSURE (TORR)

ELECTRON DENSITY (cm^{-3}) \	10	20	30	40	50	60	70	80	90	100
10^8	1.1	1.8	2.5	3.1	3.8	4.4	5.0	5.7	6.3	7.0
3×10^8	1.1	1.8	2.5	3.1	3.8	4.4	5.0	5.7	6.4	7.0
10^9	1.1	1.8	2.5	3.1	3.8	4.4	5.1	5.7	6.4	7.0
3×10^9	1.2	1.8	2.5	3.2	3.8	4.5	5.1	5.8	6.4	7.1
10^{10}	1.3	2.0	2.6	3.3	4.0	4.6	5.2	5.9	6.6	7.2
3×10^{10}	1.7	2.3	3.0	3.7	4.3	5.0	5.6	6.3	7.0	7.6
10^{11}	3.1	3.7	4.4	5.1	5.8	6.4	7.0	7.7	8.3	9.0
3×10^{11}	7.1	7.7	8.4	9.1	9.8	10	11	12	12	13
10^{12}	21	22	22	23	24	24	25	26	26	27

FIG. 9. Calculated recombination coefficient $\alpha(He_2^+)$ in a weakly ionized helium afterglow, as a function of pressure and electron density at 300 °K (in units of 10^{-9} cm^3 sec^{-1}). α is taken equal to $\alpha_2 + k_e n_e + k_{\text{He}} n_{\text{He}}$, where $\alpha_2 = 5\times10^{-10}$ cm^3 sec^{-1}, $k_e = 2\times10^{-20}$ cm^6 sec^{-1}, and $k_{\text{He}} = 2\times10^{-27}$ cm^6 sec^{-1}. n_e and n_{He} are the electron and neutral densities, respectively. The estimated error in α is 30%.

It appears that collisions with electrons and neutrals [processes (5*a*)–(5*e*), Sec. II C] play a predominant role in the determination of the recombination coefficient of weakly ionized helium plasmas (Fig. 9 gives this coefficient for different electron densities and gas pressures) and most probably in the determination of all their characteristics. The effect of neutrals is particularly noteworthy, as far as future experimental work is concerned, since it has always been neglected, even when the degree of ionization has been low.

ACKNOWLEDGMENTS

We wish to express our gratitude to Mrs. H. Jeudon and her group for important contributions to the realization of this experiment. The skill of our glassblower J. Delcher made possible the excellent performance of the vacuum system. We thank P. Fournier for his aid in obtaining data. The authors are very grateful to Professor M. Biondi for many helpful discussions and for his criticism of the manuscript.

[1]H. J. Oskam and V. R. Mittelsdadt, Phys. Rev. 132, 1445 (1963).
[2]E. E. Ferguson, F. C. Fehsenfeld, and A. L. Schmeltekopf, Phys. Rev. 138, A381 (1965).
[3]T. R. Connor and M. A. Biondi, Phys. Rev. 140, A778 (1965).
[4]G. K. Born, Phys. Rev. 169, 155 (1968).
[5]D. R. Bates and S. P. Khare, Proc. Phys. Soc. (London) 85, 231 (1965).
[6]Such a process has been already considered by Pitaevskii in 1962 [see Ref. (19)] and Thomson in 1924 [see Ref. (20)].
[7]D. R. Bates, A. E. Kingston, and R. W. P. McWhirter, Proc. Roy. Soc. (London) A267, 297 (1962).
[8]J. M. Anderson and L. Goldstein, Phys. Rev. 100, 1037 (1955).
[9]B. Sayer and J. Berlande, Phys. Letters 21, 636 (1966).
[10]R. Deloche, Eighth International Conference on Phenomena in Ionized Gases, Vienna, 1967 (unpublished); R. Deloche, C. R. Acad. Sci. Paris 266B, 664 (1968).
[11]R. Deloche and A. Gonfalone, J. Phys. 29, 27 (1968).
[12]C. B. Collins, Phys. Rev. 177, 254 (1969).
[13]H. J. Oskam and V. R. Mittelstadt, Phys. Rev. 132, 1435 (1963); D. Smith and M. J. Copsey, J. Phys. B1, 650 (1968).
[14]J. F. Delpech (private communication).
[15]D. E. Kerr, C. S. Leffel, and M. N. Hirsh (unpublished) [see Ref. (3), p. A791].
[16]L. Frommhold, M. A. Biondi, and F. J. Mehr, Phys. Rev. 165, 44 (1968).
[17]M. Gryzinski, Phys. Rev. 115, 374 (1959).
[18]We exclude of course dependence due to such processes as a change in the type of ion involved, because of collisions with neutrals.
[19]L. P. Pitaevskii, Zh. Eksperim. i Teor. Fiz. 42, 1326 (1962) [English transl.: Soviet Phys. – JETP 15, 919 (1962)].
[20]J. J. Thomson, Phil. Mag. 47, 337 (1924).
[21]H. W. Darwin, F. Emard, and H. O. Tittel [Ninth International Conference on Phenomena in Ionized Gases (unpublished)], using a different cross-section formula, find a recombination coefficient for the same mechanism three to four orders of magnitude larger than ours.
[22]We published in 1968 [R. Deloche, A. Gonfalone, and M. Cheret, C. R. Acad. Sci. Paris 267B, 934 (1968)] values of α which were slightly different (a factor of 2) from those presented here, because of approximations made in the computation of the initial electron density.
[23]C. L. Chen, C. C. Leiby, and L. Goldstein, Phys. Rev. 121, 1381 (1961).
[24]E. P. Gray, and D. E. Kerr, Bull. Am. Phys. Soc. 5, 372 (1960).

PHYSICAL REVIEW A VOLUME 1, NUMBER 3 MARCH 1970

Statistical Interpretation of London's Stress Tensor

J. Pfleiderer*
Institute for Astrophysics, University of Bonn, Bonn, Germany
(Received 15 September 1969)

London's stress tensor of the phenomenological theory of superconductivity is identified with the pressure tensor of the gas of superelectrons.

The London stresses were introduced into the phenomenological theory of superconductivity in order to balance the magnetic Maxwell stresses on a stationary supercurrent. Laue[1] has raised the question whether these stresses have physical reality or are just a convenient mathematical fiction. He proposed that they describe a force exerted by the surface of the superconductor on the supercurrent. The stresses are given by[1]

$$T_{ik}(\lambda^{1/2}j) = \lambda j_i j_k - \tfrac{1}{2}\delta_{ik}\lambda j^2 \ . \tag{1}$$

Here, j is the supercurrent, and

$$\lambda = m/e^2 n \tag{2}$$

is London's constant, with m the effective mass of superelectrons, e their charge, and n their number density. If λ is indeed a constant, one has in steady state

$$\operatorname{div} \overleftrightarrow{T}(\mu^{1/2}H) - \operatorname{div} \overleftrightarrow{T}(\lambda^{1/2}j) = 0 \ , \tag{3}$$

where $\overleftrightarrow{T}(\mu^{1/2}H)$ is Maxwell's magnetic stress tensor [written in analogy to Eq. (1)], and

$$\operatorname{div}_i \overleftrightarrow{T}(\mu^{1/2}H) = \sum \frac{\partial}{\partial x_k} T_{ik}(\mu^{1/2}H) = (\vec{j}\times\vec{B})_i \ . \tag{4}$$

If λ is varying in space (we assume that only the density n is varying, while m and e are constant), then the stationary state is given by[2]

$$\operatorname{div} \overleftrightarrow{T}(\mu^{1/2}H) - \operatorname{div} \overleftrightarrow{T}(\lambda^{1/2}j) + \tfrac{1}{2}j^2 \operatorname{grad} \lambda = 0 \ . \tag{5}$$